Coverage Analysis in the Uplink of mmWave Cellular Networks

Oluwakayode Onireti*, Ali Imran† and Muhammad Ali Imran*
*School of Engineering, University of Glasgow, Glasgow G12 8QQ, UK
†Telecommunications Engineering, University of Oklahoma, Tulsa, OK, USA
Email: {Oluwakayode.Onireti, Muhammad.Imran}@glasgow.ac.uk* and ali.imran@ou.edu†

***Abstract*—In this paper, we present an analytical framework to evaluate the coverage in the uplink of millimeter wave (mmWave) cellular networks. By using a distance dependent line-of-sight (LOS) probability function, the location of LOS and non-LOS user equipment (UE) are modeled as two independent non-homogeneous Poisson point processes, with each having different pathloss exponent. The analysis takes account of per UE fractional power control (FPC), which couples the transmission of UE due to location-dependent channel inversion. We consider the following scenarios in our analysis: 1) Pathloss based FPC (PL-FPC) which is performed using the measured pathloss and 2) Distance based FPC (D-FPC) which is performed using the measured distance. Results suggest that D-FPC outperforms the PL-FPC at high SINR. Also, the SINR coverage probability decreases as the cell density becomes greater than a threshold.**

***Index Terms*—Millimeter wave, stochastic geometry, uplink, 5G cellular networks, fractional power control.**

I. Introduction

Increasing bandwidth by moving into the millimeter wave (mmWave) band has been identified as one of the primary approaches towards meeting the data rate requirement of the fifth generation ($5\mathrm{G}$) cellular networks [1], [2]. According to [2], the available spectrum for cellular communications at the mmWave band can be easily 200 times greater than the spectrum presently allocated for this purpose below the 3 GHz [2]. The mmWave band ranging from $30-300$ GHz has already been considered for wireless services such as fixed access and personal area networking [3]. Such frequency bands have long been deemed unsuitable for cellular communications as a result of the large free space pathloss and poor penetration (i.e., blockage effect) through materials such as water, concrete, etc. Only recently, survey measurements and capacity studies of mmWave technology have revealed its promise for urban small cell deployments [1], [4]. In addition to the huge available bandwidth in mmWave band, the smaller wavelength associated with the band allows for the use of more miniaturized antennas at the same physical area of the transmitter and receiver to provide array gain [2]. With such large antenna array, the mmWave cellular system can apply beamforming at the transmit and receive sides to provide array gain which compensates for the near-field pathloss [5].

A major distinguishing factor in mmWave is the propagation environment. As a result of the blockage effect associated with mmWave, outdoor mmWave base stations (BSs) are more likely to serve outdoor user equipment (UE) since mmWave signals suffer severe penetration losses [6]. Furthermore, it has been revealed via the channel measurement in [1] that blockages results in a significant difference between the line-of-sight (LOS) and non-line-of-sight (NLOS) pathloss characteristics. The measurement showed that mmWave signal propagates with pathloss exponent of 2 in LOS path and a much higher pathloss exponent with additional shadowing in NLOS path [1]. Results in [4] showed that the achievable data rate in the mmWave system can be an order of magnitude increase over the current state-of-the-art ultra-high frequency (UHF) cellular networks. Recently, use of stochastic geometry based analysis, which has been used to analyze the rate and coverage of the conventional UHF cellular systems in [7], [8], was proposed to assess the capacity of mmWave cellular networks [9]–[12]. A stochastic blockage model, where the blockage parameters are characterized by some random distributions, was presented for mmWave cellular networks in [9]. Using the stochastic blockage process, authors in [10] proposed a framework to analyze the signal-to-interference-and-noise-ratio (SINR) coverage probability of mmWave networks in the downlink channel while considering outdoor mmWave BSs and outdoor users. In [11], a multi-slope pathloss model (where different distance ranges are subjected to different pathloss exponent), which is applicable for the mmWave model, was presented for the downlink channel. In [12], a more comprehensive analytic framework, which further incorporates self-backhauling, was presented.

In this paper, we present a stochastic geometry framework for evaluating the SINR coverage in the uplink of mmWave cellular networks with fractional power control (FPC). The aim of FPC is to minimize UE battery consumption, and minimize interference to other cells. We consider two forms of FPC:1) Pathloss based FPC (PL-FPC), which is the conventional approach and is based on the measured pathloss and 2) Distance based FPC (D-FPC), which is based on the measured distance. The rest of this paper is organized as follows: In Section II, we present the system model, detailing the stochastic blockage model and power control. In Section III, we present the stochastic geometry framework for analyzing the SINR coverage in the uplink of mmWave cellular networks with FPC. In Section IV, we present the numerical results which show that D-FPC outperforms the PL-FPC at high SINR threshold. Furthermore, the SINR coverage probability

978–1–5386–3873–6/17/$31.00

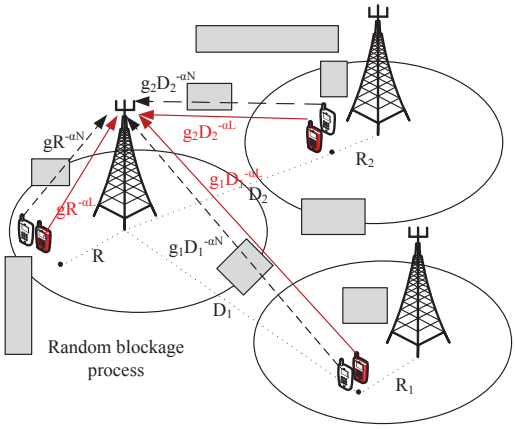

Fig. 1: Visual representation of the uplink of mmWave cellular networks, focusing on the serving UE and two interfering UE in adjacent cells. Blockages are modeled as random process of rectangles as in [10]. White and red color marked UE denotes the LOS and NLOS representation of the same UE.

decreases as the cell density becomes greater than a threshold. Finally, Section V concludes the paper.

II. System Model

We consider the uplink of a mmWave cellular network and focus on the SINR coverage experienced by outdoor users served by outdoor BSs. The outdoor BSs are spatially distributed in $\mathbb{R}^2$ according to an independent homogeneous PPP with density λ. The user location (before association) are assumed to form a realization of homogeneous PPP with density λ_u. Each BS serves a single user per channel which is randomly selected from all the users located in its Voronoi cell. Hence, the user PPP λ_u is thinned to obtain a point process $\Phi = \{X_z\}$, where X_z is the location active outdoor user. As in [13]–[15], we assume that the active users also form PPP even after associating just one user per BS. Since we have one active user per cell, the density ϕ of the thinned PPP of active users is set to be equal to the BS density λ.

The blocking effect is modeled according to [10] and we perform our analysis on a randomly chosen outdoor BS. An outdoor UE can either be LOS or NLOS to the random BS, as illustrated in Fig. 1. Let Φ_L be the point process of the LOS UEs, and Φ_N be the process of NLOS UEs. We define the LOS probability function $p(R)$ as the probability that a link of length R is LOS. The NLOS probability of the link is $1 - p(R)$. Different pathloss models are applied to the LOS and NLOS links. Hence, given a link has length R, its pathloss gain $L(R)$ can be computed as

$$L(R) = \mathbb{I}\left(p\left(R\right)\right) C_L R^{-\alpha_L} + \left(1 - \mathbb{I}\left(p\left(R\right)\right)\right) C_N R^{-\alpha_N}, \quad (1)$$

where $\mathbb{I}(r)$ is a Bernoulli random variable with parameter r, C_L and C_N are the intercepts on the LOS and NLOS pathloss expressions, α_L and α_N are the LOS and NLOS pathloss exponents. The LOS probability function is modeled from a stochastic blockage model, where the blockage is modeled as a rectangle Boolean scheme. $p(R) = e^{-\beta R}$, where β is a parameter determined by the average size and density of the blockages [9]. We assume that each UE, either LOS or NLOS, associates with the BS that offers the smallest pathloss.

Distribution of the distance between the random BS and a LOS UE: Given that a LOS UE is associated with the random BS which is at the origin, the probability distribution function (PDF) of the distance R_L between the LOS UE and its serving BS can be expressed as (2), shown at the top of the next page.

Distribution of the distance between the random BS and a NLOS UE: Given that a NLOS UE is associated with the random BS which is at the origin, the PDF of the distance R_N between a NLOS UE and its serving BS can also be expressed as (3), shown at the top of the next page.

Antenna Gain: All UEs and BSs are equipped with directional antennas with sectorized gain pattern as in [12]. The directivity gain at the random BS is taken as a constant M_r for all angles in the main lobe, and another constant m_r for the side lobes. Hence, given the beamwidth of the main lobe as θ_r, the gain function of the BS at angle ψ_r off the boresight direction can be represented by $G_{M_r,m_r,\theta_r}(\psi_r)$. In the same way, the gain function of the UE at an angle ψ_t off the boresight direction can be denoted by $G_{M_t,m_t,\theta_t}(\psi_t)$, where M_t, m_t and θ_t are the UE parameters. Here we consider that based on the estimated channel, the serving BS and the UE can adjust their beam steering angles to achieve the maximum array gains. As a result, the total directivity gain of the desired signal is $M_r M_t$. Furthermore, for the l^{th} interference link, we assume that the angle of departure at the interfering UE ψ_t^l and the angle of arrival at the random BS ψ_r^l are independently and uniformly distributed in $(0, 2\pi]$, which results in a gain of $G_l = G_{M_t,m_t,\theta_t}(\psi_t^l) G_{M_r,m_r,\theta_r}(\psi_r^l)$. Hence, the directivity gain in the interference link G_l is a discrete random variable whose probability distribution is given as a_k with probability b_k $(k \in \{1,2,3,4\})$, where $a_1 = M_r M_t$, $b_1 = \frac{\theta_r \theta_t}{4\pi^2}$, $a_2 = M_r m_t$, $b_2 = \frac{\theta_r}{2\pi}(1 - \frac{\theta_t}{2\pi})$, $a_3 = m_r M_t$, $b_3 = (1 - \frac{\theta_r}{2\pi})\frac{\theta_t}{2\pi}$, $a_4 = m_r m_t$ and $b_4 = (1 - \frac{\theta_r}{2\pi})(1 - \frac{\theta_t}{2\pi})$ [10].

UE Fractional Power Control: We assume that all UEs utilize distance-proportional FPC of the form $R^{\alpha_0 \tau}$, where $\tau \in [0,1]$ is the power control factor and α_0 is dependent on the FPC assumption. Therefore, as a UE moves closer to its associated BS, the transmit power required to achieve the target received signal power decreases. We consider two forms of FPC implementation:

1) Pathloss based FPC: PL-FPC follows the same approach as in LTE and, hence, only the pathloss which is obtained via reference signals is required for its implementation [16]. PL-FPC operates by the compensating the pathloss of the user irrespective of whether it is LOS or NLOS. Hence, $\alpha_0 = \alpha_L$ for LOS users and $\alpha_0 = \alpha_N$ for NLOS users.

2) Distance based FPC: D-FPC is based on the measured distance and always compensate by inverting with the LOS pathloss exponent, i.e., $\alpha_0 = \alpha_L$. As a result, D-FPC scheme adjusts the transmit power as if the link were LOS, even if in fact it is NLOS. The scheme requires the knowledge of the user-BS distance which can be readily obtained, since the location of the BS is known while that of the user can estimated by using GPS or position reference symbols. Note that with the PL-FPC, very few number NLOS users can result in significant performance degradation, as they will aim to compensate the NLOS path loss ($R_z^{-\alpha_N}$, where $\alpha_N \geq 4$) by transmitting high power $R_z^{\alpha_N \tau}$ thereby causing significant

$$\mathcal{F}_L(x) = \frac{2\pi\lambda x e^{-\beta x}}{\mathcal{A}_L} \exp\left(-2\pi\lambda\left(\frac{(\beta q_l x^{v_l}+1)\,e^{-\beta q_l x^{v_l}}}{\beta^2} - \frac{(\beta x+1)\,e^{-\beta x}}{\beta^2} + \frac{q_l^2 x^{2v_l}}{2}\right)\right) \quad (2)$$

where $q_l = (C_N/C_L)^{\frac{1}{\alpha_N}}$, $v_l = \alpha_L/\alpha_N$ and $\mathcal{A}_L = 2\pi\lambda\int_0^\infty x e^{-\beta x}\exp\left(-2\pi\lambda\left(\frac{(\beta q_l x^{v_l}+1)e^{-\beta q_l x^{v_l}}}{\beta^2} - \frac{(\beta x+1)e^{-\beta x}}{\beta^2} + \frac{q_l^2 x^{2v_l}}{2}\right)\right)\mathrm{d}x$ is the probability that the BS is connected to a LOS UE.

$$\mathcal{F}_N(x) = \frac{2\pi\lambda x\left(1-e^{-\beta x}\right)}{\mathcal{A}_N} \exp\left(-2\pi\lambda\left(\frac{(\beta x+1)\,e^{-\beta x}}{\beta^2} - \frac{(\beta q_n x^{v_n}+1)\,e^{-\beta q_n x^{v_n}}}{\beta^2} + \frac{x^2}{2}\right)\right) \quad (3)$$

where $q_n = (C_L/C_N)^{\frac{1}{\alpha_L}}$, $v_l = \alpha_N/\alpha_L$ and $\mathcal{A}_N = 1-\mathcal{A}_L$ is the probability that the BS is connected to a NLOS UE.

interference to other users. Such effect is avoided with the D-FPC where the transmit power remains $R_z^{\alpha_L\tau}$ with typical α_L value of 2.

Moreover, if $\tau = 0$ in either scenario, no channel inversion is performed and all users transmit with the same power.

Small Scale Fading: In order to take the significant difference in the small scale fading experienced by LOS and NLOS links into consideration, we assume independent Nakagami fading for each link. Positive integer values N_L and N_N are assumed as the the Nakagami fading parameters for the LOS and NLOS links, respectively, for simplicity. Let g_l be the small scale fading term on the l^{th} link. Then $|g_l|^2$ is a normalized gamma random variable.

Based on the earlier assumptions, the SINR received by the random BS from a UE at distance R_0 can be expressed as

$$\text{SINR} = \frac{|g_0|^2 M_r M_t L(R_0) R_0^{\alpha_0\tau}}{\sigma^2 + \sum_{l>0:X_l\in\Phi}|g_l|^2 G_l L(D_l) R_l^{\alpha_0\tau}}, \quad (4)$$

where D_l is the distance from an interfering UE to the random BS, R_l is the distance from the interfering UE to its serving BS, G_l is the directivity gain and σ^2 is the noise power.

III. SINR Coverage Probability

The SINR coverage probability $P_c(\Gamma)$ is defined as the probability that the received SINR at the random BS is above a threshold Γ, i.e., $P_c(\Gamma) = \mathbb{P}(\text{SINR} > \Gamma)$.

A. Distribution of R_z

In order to derive the SINR coverage probability expression, we first derive the distribution of the distance of any interfering UE to its serving BS. We represent the set of interfering users by $\mathcal{Z}$, the distance of an interfering user $z \in \mathcal{Z}$ to the BS of interest by D_z, and the distance of the interfering user to its serving BS by R_z. It should be noted that the random variables $\{R_z\}_{z\in\mathcal{Z}}$ are identically distributed but not independent in general. This dependence is induced by the restriction of having one user served per-BS-per channel, i.e., the coupling of the BS and served user-per channel point processes [8], [13], [14]. Here we demonstrate that this dependence is weak which motivates our independence assumption for $\{R_z\}_{z\in\mathcal{Z}}$.

As mentioned in the previous section, each BS have a single user served at any time instant. Therefore, similar to R_L and R_N, $R_{z:z\in\Phi_b}$ for $b \in \{L, N\}$ can be approximated as the distance of a randomly chosen point in $\mathbb{R}^2$, which can either be LOS or NLOS, to the BS that offers the maximum received power and hence its distribution can be approximated by

$$\begin{aligned}\mathcal{F}_{R_{zL}}(r_z) &= \mathcal{F}_{R_L}(r_z) \quad (5)\\ \mathcal{F}_{R_{zN}}(r_z) &= \mathcal{F}_{R_N}(r_z),\end{aligned}$$

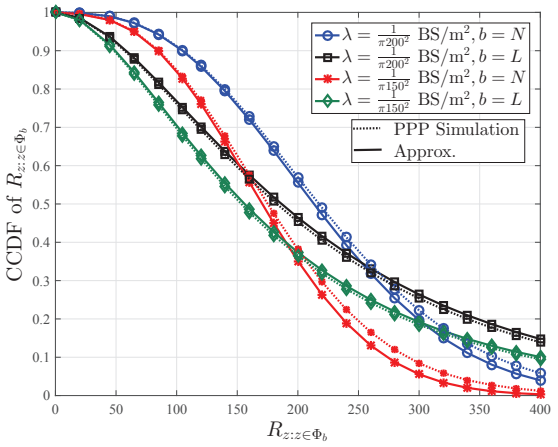

Fig. 2: A comparison of the CCDFs of $R_{z:z\in\Phi_b}$ for the PPP model with their simulation for $\lambda = \frac{1}{\pi 150^2}$ and $\frac{1}{\pi 200^2}$ BS/m^2.

where $\mathcal{F}_{R_L}(r_z)$ and $\mathcal{F}_{R_N}(r_z)$ are defined in (2) and (3), respectively. The CCDF of $R_{z:z\in\Phi_b}$ for $b \in \{L, N\}$ is given by $\mathbb{P}\left[R_{z:z\in\Phi_b} > r_z\right] = \int_{r_z}^\infty \mathcal{F}_{R_{zb}}(x)\,\mathrm{d}x$, which is shown to be a close match for the simulation of the PPP model in Fig. 2. Although Fig. 2 shows that the approximations of the distribution of R_L, R_N and $R_{z:z\in\Phi_b}$, for $b \in \{L, N\}$, are accurate, it does not give any insight into the degree of dependence between the random variables $\{R_z\}_{z\in\mathcal{Z}}$ which is defined by their joint distribution. Since it is difficult to obtain insights from the complete joint distribution of $\{R_z\}_{z\in\mathcal{Z}}$, we focus on a much simplified scenario of the joint distribution of four random variables R_{zL1}, R_{zN1}, R_{zL2} and R_{zN2}, which are the distances of LOS and NLOS users to their respective BS in the two neighboring cells. Note that since the dependence is expected to be strongest in neighboring cells, this study illustrates the worst case scenario. Hence, we numerically compute the joint pdfs $\mathcal{F}_{R_{zL1},R_{zL2}}(r_{zL1}, r_{zL2})$, $\mathcal{F}_{R_{zN1},R_{zN2}}(r_{zN1}, r_{zN2})$ and $\mathcal{F}_{R_{zL1},R_{zN2}}(r_{zL1}, r_{zN2})$ for the actual PPP model and compare them with the joint pdfs under the independence assumptions in Figs. 3, 4 and 5, respectively. The joint pdfs under the independence assumption follow directly from (2) and (3), and are given by:

$$\begin{aligned}\mathcal{F}_{R_{zL1},R_{zL2}}(r_{zL1}, r_{zL2}) &= \mathcal{F}_{R_L}(r_{zL1})\mathcal{F}_{R_L}(r_{zL2}) \quad (6)\\ \mathcal{F}_{R_{zN1},R_{zN2}}(r_{zN1}, r_{zN2}) &= \mathcal{F}_{R_N}(r_{zN1})\mathcal{F}_{R_N}(r_{zN2})\\ \mathcal{F}_{R_{zL1},R_{zN2}}(r_{zL1}, r_{zN2}) &= \mathcal{F}_{R_L}(r_{zL1})\mathcal{F}_{R_N}(r_{zN2}).\end{aligned}$$

From Figs. 3-5, we observe that the pdfs obtained from the actual PPP model and independence assumption are very similar. The correlation coefficient for $\rho_{R_{zL1},R_{zL2}}$, $\rho_{R_{N1},R_{N2}}$ and $\rho_{R_{zL1},R_{zN2}}$ are numerically computed as $0.00018, 0.0467$

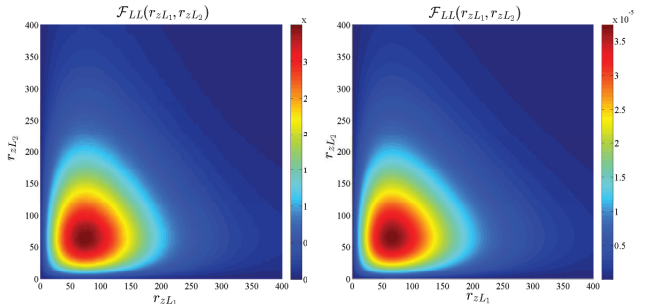

Fig. 3: Joint densities of R_{zL1} and R_{zL2} for the actual PPP model (left) and the independence assumption (right). $R_{zL1}$and R_{zL2} are the distances of LOS UEs to their respective BSs in two neighboring cells.

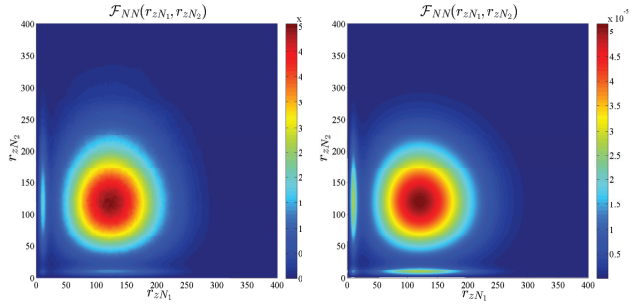

Fig. 4: Joint densities of R_{zN1} and R_{zN2} for the actual PPP model (left) and the independence assumption (right). $R_{zN1}$and R_{zN2} are the distances of LOS UEs to their respective BSs in two neighboring cells.

and -0.00137, respectively, in the simulation setup. Having validated the independence assumption, we now proceed to derive the SINR coverage probability.

B. SINR coverage probability for the case with FPC

The following theorem presents the SINR coverage probability for the PL-FPC. Modifications required for the D-FPC will be presented subsequently.

Theorem 3.1: The SINR coverage probability in the uplink of mmWave cellular networks for the case with a PL-FPC can be computed as

$$P_c\left(\Gamma\right) = \mathcal{A}_L P_{c,L}\left(\Gamma\right) + \mathcal{A}_N P_{c,N}\left(\Gamma\right), \tag{7}$$

where for $b \in \{L, N\}$, $P_{c,b}(\Gamma)$ is the conditional coverage probability given the random BS serves a user in Φ_b. Moreover, $P_{c,b}(\Gamma)$ can be obtained as

$$P_{c,L}(\Gamma) \approx \sum_{n=1}^{N_L}(-1)^{n+1}\binom{N_L}{n} \times \int_0^\infty e^{-s_L\sigma^2-\sum_{o\in\{L,N\}}(G_o(\Gamma,r)+H_o(\Gamma,r))}\mathcal{F}_{R_L}(r)\mathrm{d}r \tag{8}$$

$$P_{c,N}(\Gamma) \approx \sum_{n=1}^{N_N}(-1)^{n+1}\binom{N_N}{n} \times \int_0^\infty e^{-s_N\sigma^2-\sum_{o\in\{L,N\}}(J_o(\Gamma,r)+K_o(\Gamma,r))}\mathcal{F}_{R_N}(r)\mathrm{d}r \tag{9}$$

where

$$G_o(\Gamma,r) = -2\pi\lambda\mathcal{A}_o\sum_{k=1}^{4}b_k\int_r^\infty F\big(N_L, s_L a_k y^{\alpha_o\tau}c^{-\alpha_L}\big)ce^{-\beta c}\mathrm{d}c \tag{10}$$

$$H_o(\Gamma,r) = -2\pi\lambda\mathcal{A}_o\sum_{k=1}^{4}b_k\int_{\zeta_L(r)}^\infty F\big(N_N, s_L a_k y^{\alpha_o\tau}c^{-\alpha_N}\big)\big(1-e^{-\beta c}\big)c\mathrm{d}c$$

$$J_o(\Gamma,r) = -2\pi\lambda\mathcal{A}_o\sum_{k=1}^{4}b_k\int_{\zeta_N(r)}^\infty F\big(N_L, s_N a_k y^{\alpha_o\tau}c^{-\alpha_L}\big)\, e^{-\beta c}c\mathrm{d}c$$

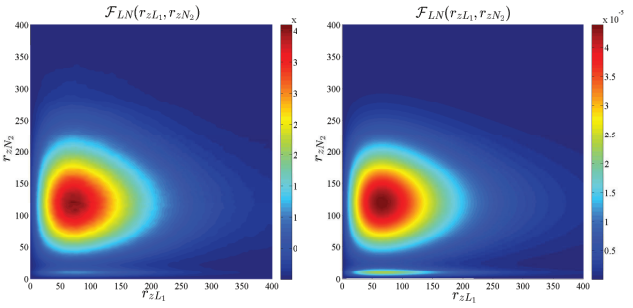

Fig. 5: Joint densities of R_{zL1} and R_{zN2} for the actual PPP model (left) and the independence assumption (right). $R_{zL1}$and R_{zN2} are the distances of LOS UEs to their respective BSs in two neighboring cells.

$$K_o(\Gamma,r) = -2\pi\lambda\mathcal{A}_o\sum_{k=1}^{4}b_k\int_r^\infty F\big(N_N, s_N a_k y^{\alpha_o\tau}c^{-\alpha_N}\big)\big(1-e^{-\beta c}\big)c\mathrm{d}c,$$

$F(N,x) = 1 - \int_0^\infty \mathcal{F}_{R_o}(y)/(1+x)^N\mathrm{d}y$, $o \in \{L, N\}$, $s_L = \frac{\eta_L n\Gamma r^{\alpha_L(1-\tau)}}{M_r M_t}$, $s_N = \frac{\eta_N n\Gamma r^{\alpha_N(1-\tau)}}{M_r M_t}$, $\zeta_L(r) = \left(\frac{C_N}{C_L}\right)^{\frac{1}{\alpha_N}} r^{\frac{\alpha_L}{\alpha_N}}$, $\zeta_N(r) = \left(\frac{C_L}{C_N}\right)^{\frac{1}{\alpha_L}} r^{\frac{\alpha_N}{\alpha_L}}$, a_k and b_k are antenna directivity parameter defined in Section II. For $s \in \{L, N\}$, $\eta_s = N_s(N_s!)^{-\frac{1}{N_s}}$ and N_s are the parameter of the Nakagami small scale fading.

Proof Given that the link between the desired user and the random BS is LOS, the conditional coverage probability can be computed as

$$P_{c,L}(\Gamma) = \int_0^\infty \mathbb{P}[\mathrm{SINR} > \Gamma]\mathcal{F}_{R_L}(r)\mathrm{d}r \tag{11}$$
$$= \int_0^\infty \mathbb{P}\left[|g_0|^2 > r^{\alpha_L(1-\tau)}\Gamma Q/(M_r M_t)\right]\mathcal{F}_{R_L}(r)\mathrm{d}r$$

where $Q = I_{LL} + I_{LN} + I_{NL} + I_{NN+}\sigma^2$, $I_{LL} = \sum_{l:X_l\in\Phi_L\cap\bar{\mathcal{B}}(0,r)\cap L}|g_l|^2 G_l D_l^{-\alpha_L} R_l^{\alpha_L\tau}$, $I_{LN} = \sum_{l:X_l\in\Phi_L\cap\bar{\mathcal{B}}(0,r)\cap N}|g_l|^2 G_l D_l^{-\alpha_L} R_l^{\alpha_N\tau}$, $I_{NL} = \sum_{l:X_l\in\Phi_N\cap\bar{\mathcal{B}}(0,\zeta_L(r))\cap L}|g_l|^2 G_l D_l^{-\alpha_N} R_l^{\alpha_L\tau}$ and $I_{NN} = \sum_{l:X_l\in\Phi_N\cap\bar{\mathcal{B}}(0,\zeta_L(r))\cap N}|g_l|^2 G_l D_l^{-\alpha_N} R_l^{\alpha_N\tau}$ are the interferences experienced at the random BS from the LOS users with LOS links to their serving BSs, LOS users with NLOS links to their serving BSs, NLOS users with LOS links to their serving BSs and NLOS users with NLOS links to their serving BSs, respectively, $\mathcal{B}(0,r)$ denotes a disc of radius r centered at the origin and $\bar{\mathcal{B}}(0,r)$ denotes outside $\mathcal{B}(0,r)$. The CCDF of the SINR at distance r from the random BS is

$$\mathbb{P}\Big[|g_0|^2 > r^{\alpha L(1-\tau)}\Gamma Q/(M_r M_t)\Big] \tag{12}$$
$$\overset{(a)}{\approx} 1 - \mathbb{E}_\Phi\left[\left(1 - e^{\left(-\eta_L r^{\alpha_L(1-\tau)}\Gamma Q/(M_r M_t)\right)}\right)^{N_L}\right]$$
$$\overset{(b)}{=} \sum_{n=1}^{N_L}(-1)^{n+1}\binom{N_L}{n}\mathbb{E}_\Phi\left[e^{\left(-\eta_L n r^{\alpha_L(1-\tau)}\Gamma Q/(M_r M_t)\right)}\right]$$
$$\overset{(c)}{=} \sum_{n=1}^{N_L}(-1)^{n+1}\binom{N_L}{n}e^{\left(-s_L\sigma^2\right)}\prod_{i,j\in L,N}\mathcal{L}_{I_{i,j}}(s_L)$$

where $s_L = \frac{\eta_L n r^{\alpha_L(1-\tau)}\Gamma}{M_r M_t}$, $\eta_L = N_L(N_L!)^{-\frac{1}{N_L}}$, (a) follow from the fact that $|g_0|^2$ is a normalized gamma random variable with parameter N_L and the fact that for a constant $\gamma > 0$, the probability $\mathbb{P}(|g_0|^2 < \gamma)$ is tightly upper bounded by

$\left[1-\exp\left(-\gamma N_L\left(N_L!\right)^{-\frac{1}{N_L}}\right)\right]^{N_L}$ [17]. (b) follows from the binomial theorem and the earlier assumption that N_L is a positive integer, and (c) follows from the definition of Laplace transform of interference $\mathcal{L}_{I_{i,j}}(s_L) = \mathbb{E}_{I_{i,j}}\left[e^{-s_L I_{i,j}}\right]$. To complete the derivation, stochastic geometry concepts can be applied to derive the expression for $\mathcal{L}_{I_{LL}}(s_L)$ in (12) as

$$\begin{aligned}
&\mathcal{L}_{I_{LL}}(s_L) = \mathbb{E}_{I_{LL}}[e^{-s_L I_{LL}}] \\
&= \mathbb{E}_{\Phi_L}\left[\exp\left\{-s_L \sum_{z:X_z\in\Phi_L\cap\bar{\mathcal{B}}(0,r)\cap L} |g_z|^2 G_z D_z^{-\alpha_L} R_z^{\alpha_L\tau}\right\}\right] \\
&= \mathbb{E}_{R_z,G_z,D_z,g_z}\left[\prod_{z:X_z\in\Phi_L\cap\bar{\mathcal{B}}(0,r)\cap L} \exp\left\{-s_L|g_z|^2 G_z D_z^{-\alpha_L} R_z^{\alpha_L\tau}\right\}\right] \\
&\overset{(d)}{=} e^{\left(-2\pi\lambda\mathcal{A}_L\sum_{k=1}^{4} b_k\int_r^\infty e^{-\beta c}\left(1-\mathbb{E}_{R_z,g}\left[\exp\left\{-s_L g c^{-\alpha_L} R_z^{\alpha_L\tau}\right\}\right]\right)c\mathrm{d}c\right)} \\
&\overset{(e)}{=} e^{\left(-2\pi\lambda\mathcal{A}_L\sum_{k=1}^{4} b_k\int_r^\infty e^{-\beta c}\left(1-\mathbb{E}_{R_z}\left[\frac{1}{1+s_L a_k c^{-\alpha_L} R_z^{\alpha_L\tau}}\right]^{N_L}\right)c\mathrm{d}c\right)} \\
&\overset{(f)}{=} \prod_{k=1}^{4} e^{\left(-2\pi\lambda\mathcal{A}_L b_k\int_r^\infty e^{-\beta c}\left(1-\int_0^\infty \frac{\mathcal{F}_{R_L}(y)}{(1+s_L a_k c^{-\alpha_L} y^{\alpha_L\tau})^{N_L}}\mathrm{d}y\right)c\mathrm{d}c\right)} \\
&= e^{-G_L(\Gamma,r)},
\end{aligned}$$

where g in (d) is a normalized gamma variable with parameter N_L, a_k and b_k are defined in earlier in Section II, (d) follows from the probability generating functional of the PPP [7], and the independence of the interference link directivity gain G_z with probability distribution $G_z = a_k$ with probability b_k. Furthermore, λ is thinned by $\mathcal{A}_L$ to capture R_z that are LOS to their serving BS. (e) follows from computing the moment generating function of a gamma random variable g, and (f) follows from the independence of $\{R_z\}_{z\in\mathcal{Z}}$ which has been validated earlier in Section III-A and the fact that the interfering users are in LOS to their serving BS. The computation for $\mathcal{L}_{I_{LN}}(s_L)$ which denotes the Laplace transform of LOS interfering links with NLOS links to their serving BS can be obtained by following the same process such that,

$$\begin{aligned}
&\mathcal{L}_{I_{LN}}(s_L) = \mathbb{E}_{I_{LN}}[e^{-s_L I_{LN}}] \qquad (13)\\
&= \prod_{k=1}^{4} e^{\left(-2\pi\lambda\mathcal{A}_N b_k\int_r^\infty e^{-\beta c}\left(1-\int_0^\infty \frac{\mathcal{F}_{R_N}(y)}{(1+s_L a_k c^{-\alpha_L} y^{\alpha_N\tau})^{N_L}}\mathrm{d}y\right)c\mathrm{d}c\right)} \\
&= e^{-G_N(\Gamma,r)}.
\end{aligned}$$

Similarly, for the NLOS interfering links which are in LOS to their serving BS, $\mathcal{L}_{I_{NL}}(s_L)$ in (12) can be computed as

$$\begin{aligned}
&\mathcal{L}_{I_{NL}}(s_l) \quad = \mathbb{E}_{I_{NL}}[e^{-s_L I_{NL}}] \qquad (14)\\
&= \mathbb{E}_{\Phi_N}\left[\exp\left\{-s_L \sum_{z:X_z\in\Phi_L\cap\bar{\mathcal{B}}(0,\zeta_L(r))\cap L} |g_z|^2 G_z D_z^{-\alpha_N} R_z^{\alpha_L\tau}\right\}\right] \\
&= \prod_{k=1}^{4} e^{\left(-2\pi\lambda\mathcal{A}_L b_k\int_{\zeta_L(r)}^\infty (1-e^{-\beta c})\left(1-\int_0^\infty \frac{\mathcal{F}_{R_L}(y)}{(1+s_L a_k c^{-\alpha_N} y^{\alpha_L\tau})^{N_N}}\mathrm{d}y\right)c\mathrm{d}c\right)} \\
&= e^{-H_L(\Gamma,r)}.
\end{aligned}$$

Furthermore, for NLOS interfering links which are NLOS to their serving BS, $\mathcal{L}_{I_{NN}}(s_L)$ in (12) can be computed as

$$\begin{aligned}
&\mathcal{L}_{I_{NN}}(s_L) \quad = \mathbb{E}_{I_{NN}}[e^{-s_L I_{NN}}] \qquad (15)\\
&= \prod_{k=1}^{4} e^{\left(-2\pi\lambda\mathcal{A}_N b_k\int_{\zeta_L(r)}^\infty (1-e^{-\beta c})\left(1-\int_0^\infty \frac{\mathcal{F}_{R_N}(y)}{(1+s_L a_k c^{-\alpha_N} y^{\alpha_N\tau})^{N_N}}\mathrm{d}y\right)c\mathrm{d}c\right)} \\
&= e^{-H_N(\Gamma,r)}
\end{aligned}$$

Hence, we obtain (8) by substituting for $\mathcal{L}_{I_{i,j}}(s_L)$ in (12), which is further substituted into (11).

Given that the link between the desired user and the random BS is NLOS, we can also compute the conditional probability $P_{c,N}(\Gamma)$ by following the same approach as that of $P_{c,L}(\Gamma)$. Thus we omit the detailed proof of (9) here.

Consequently, from the law of total probability, it follows that $P_c(\Gamma) = \mathcal{A}_L P_{c,L}(\Gamma) + \mathcal{A}_N P_{c,N}(\Gamma)$.

Corollary 3.2: The SINR coverage probability in the uplink of mmWave cellular networks for the case with D-FPC can be computed as in (7) but with $\alpha_o = \alpha_L$ and $s_N = \frac{\eta_N n\Gamma r^{\alpha_N-\alpha_L\tau}}{M_r M_t}$ in (10).

IV. Numerical Results and Discussion

In this section, we present some numerical results to illustrate our analytical findings in Section III. We assume that the mmWave network is operated at 28 GHz with 100 MHz allocated to each UE. The LOS and NLOS pathloss exponents are taken as $\alpha_L = 2$ and $\alpha_N = 4$ while the Nakagami fading parameters are $N_L = 3$ and $N_N = 2$. Furthermore, we assume the LOS probability function $p(R) = e^{-\beta R}$, where $1/\beta = 141.4$ m. For comparison purpose, we have also included the conventional stochastic geometry analysis of the uplink channel in [8] that does not differentiate between LOS and NLOS transmission, and assumes small-scale Rayleigh fading between the UEs and BSs (i.e., $N_L = N_N = 1$). Note that only one pathloss exponent is defined in [8], and is denoted here as $\alpha = \alpha_N$.

In Fig. 6a, we compare the SINR coverage probability obtained via our analytical framework in Theorem 3.1 with the Monte Carlo simulations for FPC factor $\tau = 0$. Results in Fig. 6a show that our analytical results in Theorem 3.1 closely match with the simulation results. Though the gap between derived expressions and simulation results stays small for all tested scenarios, this gap becomes negligible as density of BS grows. As future mmWave networks are expected to have high BS density, the derived expressions provide highly accurate method to estimate uplink coverage probability for mmWave networks. Note that the analytical results are based on the independence assumption and, hence, the results in Fig. 6a further validates the accuracy of the independence assumption presented earlier in Figs. 3-5.

In Figs. 6b and 6c, we plot the SINR coverage distribution obtained from our analytical framework as a function of the BS density for the case with no power control, i.e. $\tau = 0$, and full power control (PL-FPC and D-FPC), i.e. $\tau = 1$, respectively. The plots in Fig. 6b are also benchmarked with the results obtained from the conventional stochastic geometry analysis for the uplink channel in [8]. For the case without power control ($\tau = 0$) in Fig. 6(b), the coverage probability performance obtained from the conventional stochastic geometry analysis in [8], initially increases with the BS density. This is due to the fact that having more BSs leads to improved coverage in the noise limited network (i.e. eliminates coverage hole). When λ is large enough (e.g., $\lambda > 10^{-1}$ BSs/km^2), the SINR coverage probability becomes independent of the BS density as the network becomes interference limited. The simple pathloss model is responsible for this behaviour as the increased interference is being counterbalanced by the increase

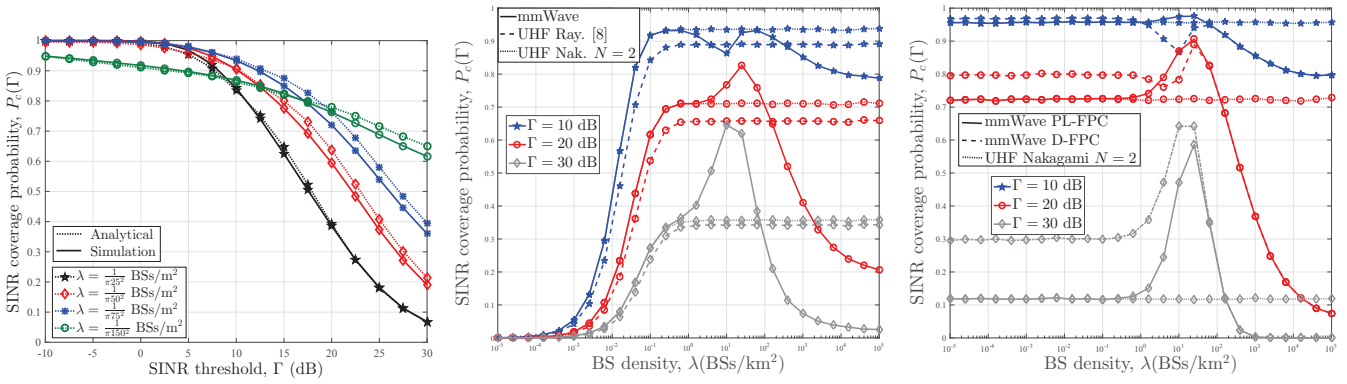

(a) Accuracy of analytical framework, $\tau = 0$ (b) Comparison with the UHF network for $\tau = 0$ (c) Comparison with the UHF network for $\tau = 1$

Fig. 6: SINR coverage probability in the uplink channel with $M_r = M_t = 10$ dB, $m_r = m_t = -10$ dB, $\theta_t = 90°$ and $\theta_r = 30°$.

in the signal power as λ increases in the interference limited network. In the mmWave framework, the same observation, which follows the conventional analysis, is experienced in the noised limited region. However, when the mmWave network becomes denser than a certain threshold, the coverage probability starts decreasing. The reason behind this is that NLOS interference paths are converted to LOS interference paths.

For the case with full power control, increasing the BS density does not have any impact on the SINR coverage probability obtained from the conventional framework. On the contrary, the coverage probability of the mmWave framework with PL-FPC remains the same with increasing BS density until a threshold where it start rising to its peak, and then decreases afterwards. Implementing the distance dependent full power control for the conventional framework implies that the transmit power of all users reduces as the BS density increases and hence, the SINR coverage probability remains unaffected. Whereas as NLOS paths converts to LOS paths in the mmWave framework with PL-FPC, the resultant interference initially reduces causing the SINR coverage to increase. Further increase in BS density leads to a sharp fall in the coverage as the users paths becomes LOS. Regarding the D-FPC, it outperforms the PL-FPC at low BS density and converges to the PL-FPC at high BS density. This convergence is expected since all path becomes LOS at very high BS density. Furthermore, for the UHF network with Nakagami fading, it can be observed that its SINR coverage probability converges to that of mmWave with when there is no power control and $\lambda < 10^{-0.2}\text{BS}/\text{km}^2$. Similar observation can be seen for the PL-FPC with full power control.

V. Conclusions

In this paper, we have presented a stochastic geometry framework to analyze the coverage in the uplink of millimeter wave cellular networks. The framework takes the effect of blockage into consideration by utilizing a distance dependent line-of-sight probability function, and modeling the location of LOS and non-LOS users as two independent non-homogeneous Poisson point processes. The proposed model takes into account per user fractional power control, which couples the transmission of users due to location-dependent channel inversion. The numerical results show that there exists a finite number of mmWave base stations that maximizes the SINR coverage probability.

Acknowledgment

We acknowledge the support of EPSRC (GCRF) funds under the grant no. EP/P028764/1

References

[1] T. Rappaport et al., "Millimeter wave mobile communications for 5G cellular: It will work!" *IEEE Access*, vol. 1, pp. 335–349, 2013.
[2] Z. Pi and F. Khan, "An Introduction to Millimeter-Wave Mobile Broadband Systems," *IEEE Commun. Mag.*, vol. 49, pp. 101–107, Jun. 2011.
[3] *IEEE Standard for WirelessMAN-Advanced Air Interface for Broadband Wireless Access Systems*, 2012.
[4] M. Akdeniz et al., "Millimeter wave channel modeling and cellular capacity evaluation," *IEEE J. Sel. Areas Commun.*, vol. 32, no. 6, pp. 1164–1179, Jun. 2014.
[5] W. Roh et al., "Millimeter-wave beamforming as an enabling technology for 5G cellular communications: Theoretical feasibility and prototype results," *IEEE Commun. Mag.*, vol. 52, no. 2, pp. 106–113, Feb. 2014.
[6] A. Alejos et al., "Measurement and analysis of propagation mechanisms at 40 GHz: Viability of site shielding forced by obstacles," *IEEE Trans. Veh. Technol.*, vol. 57, no. 6, pp. 3369–3380, Nov. 2008.
[7] J. Andrews, F. Baccelli, and R. Ganti, "A tractable approach to coverage and rate in cellular networks," *IEEE Trans. Commun.*, vol. 59, no. 11, pp. 3122–3134, Nov. 2011.
[8] T. Novlan, H. Dhillon, and J. Andrews, "Analytical modeling of uplink cellular networks," *IEEE Trans. Wireless Commun.*, vol. 12, no. 6, pp. 2669–2679, Jun. 2013.
[9] T. Bai, R. Vaze, and R. Heath, "Analysis of blockage effects on urban cellular networks," *IEEE Trans. Wireless Commun.*, vol. 13, no. 9, pp. 5070–5083, Sep. 2014.
[10] T. Bai and R. Heath, "Coverage and rate analysis for millimeter-wave cellular networks," *IEEE Trans. Wireless Commun.*, vol. 14, no. 2, pp. 1100–1114, Feb. 2015.
[11] M. Ding et al., "Will the area spectral efficiency monotonically grow as small cells go dense?" in *IEEE Globecom*, San Diego USA, Dec 2015.
[12] S. Singh, M. Kulkarni, A. Ghosh, and J. Andrews, "Tractable model for rate in self-backhauled millimeter wave cellular networks," *IEEE J. Sel. Areas Commun.*, vol. 33, no. 10, pp. 2196–2211, Oct. 2015.
[13] J. Andrews, A. K. Gupta, and H. S. Dhillon, "A primer on cellular network analysis using stochastic geometry," *submitted to IEEE Access 2016*, available online: https://arxiv.org/pdf/1604.03183v2.pdf.
[14] H. ElSawy and E. Hossain, "On stochastic geometry modeling of cellular uplink transmission with truncated channel inversion power control," *IEEE Trans. Wireless Commun.*, vol. 13, pp. 4454–4469, 2014.
[15] O. Onireti, A. Imran, M. A. Imran, and R. Tafazolli, "Energy efficient inter-frequency small cell discovery in heterogeneous networks," *IEEE Trans. Veh. Technol.*, vol. 65, no. 9, pp. 7122–7135, Sept. 2016.
[16] A. Simonsson and A. Furuskar, "Uplink power control in LTE - overview and performance, subtitle: Principles and benefits of utilizing rather than compensating for SINR variations," in *IEEE VTC-Fall*, 2008, pp. 1–5.
[17] H. Alzer, "On some inequalities for the incomplete gamma function," *Math. Comput.*, vol. 66, no. 218, pp. 771–778, Apr. 1997.